Published in final edited form as:
Exp Neurol. 2013 October ; 248: 157–169. doi:10.1016/j.expneurol.2013.06.011.

Paxillin phosphorylation counteracts proteoglycan-mediated inhibition of axon regeneration

Tomoharu Kuboyama[a,b], **Xueting Luo**[c], **Kevin Park**[c], **Murray G. Blackmore**[c,d], **Takuro Tojima**[a,e], **Chihiro Tohda**[b], **John L. Bixby**[c], **Vance P. Lemmon**[c], and **Hiroyuki Kamiguchi**[a,*]

[a]Laboratory for Neuronal Growth Mechanisms, RIKEN Brain Science Institute, Wako, Saitama 351-0198, Japan

[b]Division of Neuromedical Science, Institute of Natural Medicine, University of Toyama, Toyama, Toyama 930-0194, Japan

[c]The Miami Project to Cure Paralysis, Department of Neurological Surgery, University of Miami, Miami, FL 33136, USA

[d]Department of Biomedical Sciences, Marquette University, Milwaukee, WI 53201, USA

[e]PRESTO, Japan Science and Technology Agency, Kawaguchi, Saitama 332-0012, Japan

Abstract

In the adult central nervous system, the tips of axons severed by injury are commonly transformed into dystrophic endballs and cease migration upon encountering a rising concentration gradient of inhibitory proteoglycans. However, intracellular signaling networks mediating endball migration failure remain largely unknown. Here we show that manipulation of protein kinase A (PKA) or its downstream adhesion component paxillin can reactivate the locomotive machinery of endballs *in vitro* and facilitate axon growth after injury *in vivo*. In dissociated cultures of adult rat dorsal root ganglion neurons, PKA is activated in endballs formed on gradients of the inhibitory proteoglycan aggrecan, and pharmacological inhibition of PKA promotes axon growth on aggrecan gradients most likely through phosphorylation of paxillin at serine 301. Remarkably, pre-formed endballs on aggrecan gradients resume forward migration in response to PKA inhibition. This resumption of endball migration is associated with increased turnover of adhesive point contacts dependent upon paxillin phosphorylation. Furthermore, expression of phosphomimetic paxillin overcomes aggrecan-mediated growth arrest of endballs, and facilitates axon growth after optic nerve crush *in vivo*. These results point to the importance of adhesion dynamics in restoring endball migration and suggest a potential therapeutic target for axon tract repair.

Keywords

Aggrecan; Axon regeneration; Dystrophic endball; Optic nerve; p21-activated kinase; Paxillin; Point contact; Protein kinase A

*Corresponding author: Hiroyuki Kamiguchi, RIKEN Brain Science Institute, 2-1 Hirosawa, Wako, Saitama 351-0198, Japan, Phone: +81-48-467-6137; Fax: +81-48-467-9795, kamiguchi@brain.riken.jp.

Introduction

After neuronal networks have developed, injury to the adult central nervous system (CNS) induces the formation of glial scars and myelin debris that release or expose many inhibitors of axon regeneration (Yiu and He, 2006). Glial scars formed in the vicinity of injured regions consist predominantly of reactive astrocytes together with other cell types that secrete inhibitory proteoglycans such as chondroitin sulfate proteoglycans (CSPG) and keratan sulfate proteoglycans (KSPG). These proteoglycans pose a major impediment to axon regeneration (Bradbury et al., 2002; Imagama et al., 2011; Jones and Tuszynski, 2002; McKeon et al., 1991; Silver and Miller, 2004). CSPG receptors include two Type IIa receptor protein tyrosine phosphatases (RPTPs) as well as Nogo receptors (Dickendesher et al., 2012; Fisher et al., 2011; Fry et al., 2010; Shen et al., 2009). Because Type IIa RPTPs also interact with heparan sulfate proteoglycans (Aricescu et al., 2002; Johnson et al., 2006) that facilitate axon growth (Bandtlow and Zimmermann, 2000; Van Vactor et al., 2006), targeting receptor-downstream events specific to inhibitory proteoglycans is a reasonable strategy for axon tract repair after CNS injury. However, the intracellular signal transduction networks mediating CSPG-based inhibition of axon regeneration are largely unknown.

After CNS injury, the inhibitory proteoglycans CSPG and KSPG are organized as a gradient with higher concentration in the lesion core and lower in the penumbra (Davies et al., 1999; Ito et al., 2010; Jones and Tuszynski, 2002; Silver and Miller, 2004). As the tips of regenerating axons approach the injury site, they migrate into the penumbra but eventually stop advancing and become swollen into “dystrophic endballs” in the rising gradient of inhibitory proteoglycans. Ramón y Cajal first described this dystrophic structure and believed that it was a final resting state of the immobilized axon tip (Ramón y Cajal, 1928). However, *in vitro* reproduction of dystrophic endballs on a gradient of aggrecan, an inhibitory proteoglycan that contains chondroitin sulfate and keratan sulfate chains, revealed that endballs are highly motile for some time but incapable of forward translocation in this hostile environment (Tom et al., 2004). This finding suggests that axon growth on proteoglycan gradients *in vitro* and possibly across glial scars *in vivo* is achievable if we can properly manipulate intracellular molecular machinery for endball migration. Although *in vitro* searches so far have failed to identify compounds that restore the capability of endballs to grow robustly on aggrecan gradients (Steinmetz et al., 2005), we report here that endballs can resume forward migration in this hostile environment after pharmacological or genetic perturbation that induces serine phosphorylation on paxillin, an intracellular component of the adhesion machinery. We also show that chemical induction or genetic mimicking of paxillin phosphorylation is sufficient to overcome aggrecan-mediated growth arrest of endballs *in vitro* and to facilitate axon growth in the injured adult CNS *in vivo*, possibly through activation of adhesion turnover in endballs.

Materials and methods

cDNA constructs

Rat paxillin cDNA (clone ID: 7128801) was purchased from Open Biosystems. Rat p21-activated kinase 1 (PAK1) cDNA was obtained through RT-PCR of total brain RNA derived from embryonic day 18 Wister rat (SLC) using the following primer pair: 5′-ACGCGTCGACGCCACCATGTCAAATAACGGCTTAGACG-3′ and 5′-ATGTTTAGCGGCCGCCAGGAAATGGGAGAAGCAAG-3′. These cDNAs were subcloned into pCAGGS, a mammalian expression vector under the control of the CAG promoter (provided by J. Miyazaki, Osaka University, Suita, Osaka, Japan) (Niwa et al., 1991). cDNAs encoding for the following fluorescent proteins were inserted into the vectors adjacent to the 3′ end of paxillin cDNA or adjacent to the 5′ end of PAK1 cDNA: Venus (provided by A. Miyawaki, RIKEN Brain Science Institute, Wako, Saitama, Japan) (Nagai

et al., 2002) and TagRFP-T (Shaner et al., 2008), a modified version of TagRFP (Evrogen). Single amino acid mutations were introduced into paxillin and PAK1 sequences using QuickChange II Site-Directed Mutagenesis Kit (Agilent Technologies) according to the manufacturer's protocol.

Cell culture substrates

Glass-based dishes were coated with 0.1% poly-D-lysine (PDL, Sigma) overnight at 37°C. An uniform substrate of laminin or aggrecan was prepared by incubating PDL-coated glass coverslips with 10 μg/ml laminin (Invitrogen) or 10 μg/ml laminin plus 200 μg/ml aggrecan (Sigma), respectively, in calcium and magnesium-free Hanks' balanced salt solution (Invitrogen) for 3 h at 37°C. A gradient substrate of aggrecan was prepared as described previously (Tom et al., 2004) with minor modifications. Briefly, PDL-coated coverslips were spotted with 2 μl of a solution of 1.6 mg/ml aggrecan and 10 μg/ml laminin. This procedure caused a circular area of approximately 2.2 mm in diameter to be coated with aggrecan, in which the rim of the circle contained increasingly higher concentrations of aggrecan than the center. After the spots were air dried, the coverslips were completely covered with 10 μg/ml laminin.

Neuronal culture

Dorsal root ganglions (DRGs) of adult Sprague-Dawley rat (200-240 g, female, SLC) were dissociated and cultured as described previously (Tom et al., 2004). Briefly, DRGs were dissociated with 2.5 units/ml dispase II (Roche) and 200 units/ml collagenase type 2 (Worthington) for 70 min at 35°C. Neuronal cultures were maintained in Neurobasal-A medium (Invitrogen) containing 2% B-27 (Invitrogen), 1% Glutamax (Invitrogen) and 1% Antibiotic-Antimycotic liquid (Invitrogen) in a humidified atmosphere of 5% CO_2 at 37°C. During live cell imaging, neuronal cultures were maintained in Leibovitz's L-15 medium (Invitrogen) supplemented with 2% B-27 in a humidified atmosphere of 100% air at 37°C. For gene transfection, dissociated DRG neurons were nucleofected using Nucleofector II (Lonza) according to the manufacturer's protocol G-013.

Quantification of axon growth in vitro

Axon crossing of aggrecan gradients was evaluated by measuring the total length of axons in the aggrecan rim. Four hours after plating DRG neurons on spot preparations, the cells were treated with the following compounds: 20 μM forskolin (adenylate cyclase activator, Sigma), 20 μM Sp-cAMPS (cAMP analog, Calbiochem), 10 μM 8-(4-chlorophenylthio)-2′-O-methyladenosine-3′,5′-cyclic monophosphate (8-CPT-2′-O-Me-cAMP, Epac activator, Biolog), 10 μM N^6-benzoyladenosine-3′,5′-cyclic monophosphate [6-Bnz-cAMP, protein kinase A (PKA) activator, Biolog], 1 μM KT5720 (PKA inhibitor, Calbiochem), 100 μM myristoylated protein kinase inhibitor-(14-22)-amide (mPKI, PKA inhibitor, BioMol), 20 μM 8-bromo-cGMP (8-Br-cGMP, cGMP analog, Calbiochem), 1 μM KT5823 (protein kinase G inhibitor, Calbiochem), 50 μM 1-Hydroxy-2-oxo-3,3-bis(2-aminoethyl)-1-triazene (NOC18, nitric oxide donor, Dojindo), 50 μM 2-(4-carboxyphenyl)-4,4,5,5-tetramethylimidazoline-1-oxyl-3-oxide (PTIO, nitric oxide scavenger, Calbiochem), 100 nM AG1478 (epidermal growth factor receptor inhibitor, Sigma), 100 nM PD168393 (epidermal growth factor receptor inhibitor, Calbiochem), 1 μM KN93 (calcium/calmodulin-dependent protein kinase inhibitor, Sigma), 100 nM phorbol 12-myristate 13-acetate (protein kinase C activator, Wako), 1 μM Gö6976 (protein kinase C inhibitor, LC laboratories), 100 nM wortmannin (phosphoinositide 3-kinase inhibitor, Calbiochem), 20 μM PD98059 (mitogen-activated protein kinase kinase inhibitor, Santa Cruz), 100 μM $NiCl_2$ (voltage-gated calcium channel blocker, Wako), 10 μM tetrodotoxin (sodium channel blocker, Alomone Labs), 10 nM paclitaxel (microtubule stabilizer, Calbiochem), 0.69 U/ml chondroitinase ABC, (Seikagaku Corporation).

Two days after gene transfection and/or pharmacological treatment, the cells were fixed and immunostained with rabbit anti-β tubulin III IgG (1:1000 dilution, Sigma, catalog No. T2200) and Alexa Fluor 594-conjugated anti-rabbit IgG (1:400 dilution, Invitrogen). Transfected cells were identified by Venus or TagRFP-T fluorescence. Aggrecan gradients were visualized with mouse anti-chondroitin sulfate IgM (clone CS-56, 1:500 dilution, Sigma) and Alexa Fluor 350-conjugated anti-mouse IgM (1:400 dilution, Invitrogen). The cells were observed with a 10× NA 0.40 objective lens (UPlanSApo, Olympus) on an inverted microscope (IX81, Olympus). Fluorescence images were acquired with a cooled charge coupled device (CCD) camera (ORCA-AG, Hamamatsu Photonics, binning set at 2×2) under the control of SlideBook software (Roper). The outer boundary of aggrecan rims was identified on the CS-56 fluorescence image, and an inner rim boundary was set at 120 μm distant from the outer boundary such that aggrecan rims on all images have the equal width. Then, the total length of axons in the aggrecan rim was defined as the sum of lengths of all axonal segments located between the outer and inner boundaries. The measurements were performed using ImageJ software (National Institutes of Health).

Axon growth on uniform substrates was assessed by measuring the length of the longest axon in each neuron. Four hours after plating, DRG neurons were treated with 1 μM KT5720 or vehicle only. After an additional 20-h incubation, the cells were immunolabeled for β tubulin III and subjected to axon length measurements as described previously (Kamiguchi and Yoshihara, 2001).

Quantification of endball migration in vitro

Endball migration was quantified two days after plating on aggrecan spot preparations. DIC images of dystrophic endballs were acquired every 1 min with a 100× NA 1.40 oil objective lens (UPlanSApo, Olympus) and a CCD camera (ORCA-AG, binning set at 2×2) on an inverted microscope (IX81). Migration speed was determined by measuring displacement of an endball tip using SlideBook software.

Protein kinase A immunofluorescence

Two days after plating, DRG neurons were pharmacologically treated for 5 min and then processed for PKA immunofluorescence using mouse IgG against PKA regulatory subunit II (RII) (1:400 dilution, BD Biosciences, catalog No. 612242) and rabbit IgG against PKA RII phosphorylated at serine 96 (pS^{96} PKA RII) (1:200 dilution, Epitomics, catalog No. 1151-1). Binding of these primary antibodies was visualized with Alexa Fluor 488-conjugated anti-mouse IgG (1:400 dilution, Invitrogen) and Alexa Fluor 594-conjugated anti-rabbit IgG (1:400 dilution, Invitrogen). The cells were observed with a 63× NA 1.40 oil objective lens (Plan-Apochromat, Carl Zeiss) and a CCD camera (AxioCam MRm, Carl Zeiss, binning set at 1×1) on an inverted microscope (Axio Observer Z1, Carl Zeiss). The outline of growth cones or endballs was determined manually, and background-subtracted fluorescence signals in the region of interest were quantified using AxioVision software (Carl Zeiss).

Western blotting

Two days after plating on uniform laminin, DRG neurons were treated for 5 min with 1 μM KT5720 or vehicle only, and then lysed in RIPA buffer [20 mM Tris (pH 7.4), 150 mM NaCl, 2 mM EDTA, 1% NP-40, 1% sodium deoxycholate, 0.1% SDS, PhosSTOP Phosphatase inhibitor cocktail (Roche), EDTA-free protease inhibitor cocktail (Roche)]. Ten micrograms of proteins were heat-denatured, electrophoresed in a 2-15% SDS-polyacrylamide gradient gel and transferred onto a polyvinylidene difluoride membrane. After blocking with Tris-buffered saline containing 2% skim milk and 0.1% Tween 20, the membrane was incubated with rabbit IgG that recognizes paxillin phosphorylated at serine 301 (pS^{301} paxillin) (1:1,000 dilution, Invitrogen, catalog No. 44-1028G) and horseradish

peroxidase (HRP)-conjugated secondary antibody (Amersham). The blots were visualized with Immobilon Western Chemiluminescent HRP substrate (Millipore), and their intensities were quantified using ImageJ software. The blots were then stripped using WB Stripping Solution (Nakarai Tesque), reprobed with mouse anti-paxillin IgG (1:50,000, BD Biosciences, catalog No. 610051) and HRP-conjugated secondary antibody, and processed for intensity quantification.

Total internal reflection fluorescence imaging

Neurons were observed under an inverted microscope (IX81) equipped with a total internal reflection illumination system (IX2-RFAEVA-2, Olympus) and a 100× NA 1.45 oil objective lens (PlanApo TIRFM, Olympus). Paxillin-TagRFP-T was excited with a 561 nm solid-state laser (LASOS Lasertechnik), and total internal reflection fluorescence (TIRF) images were collected through a long-pass filter (LP02-568RS, Semrock) and acquired every 20 s with a CCD camera (ORCA-AG, binning set at 2×2) under the control of MetaMorph software (Molecular Devices). As described previously (Woo and Gomez, 2006), we defined adhesive point contacts as immobile paxillin accumulations that showed at least 25% brighter fluorescence than the surrounding background. We also defined the lifetime of point contacts as duration between their appearance and disappearance. This analysis included all point contacts that appeared and disappeared in axon endings during observation periods.

Virus construction and production

Adeno-associated virus 2 (AAV2)-GFP was described previously (Park et al., 2008). For AAV2-S301D paxillin-FLAG, S301D paxillin was PCR-amplified from the pCAGGS construct described above using primers that incorporated a 5′ Xho1 restriction site and a 3′ 3× FLAG epitope and EcoR1 restriction site: 5′-GAATTCATCTACCATGGACTACAAAGACCATGACGGTGATTATAAAGATCATGACATCGATTACAAGGATGACGATGACAAGATGGACGACCTCGACGCC-3′ and 5′-CTCGAGCTAACAGAAGAGCTTCAGGAAGC-3′. The amplified product was then digested and ligated into pAAV-MCS plasmid (Stratagene) between EcoR1 and Xho1. AAV2 viral particles were prepared by the University of Miami Viral Vector Core using a fast protein liquid chromatography method to produce titers of approximately 4×10^{13} particles/ml.

Eye surgery, intravitreal injection and optic nerve injury

All experimental procedures were performed in compliance with animal protocols approved by the IACUC at University of Miami Miller School of Medicine. For all surgical procedures, mice were anaesthetized with ketamine and xylazine. Eye ointment containing atropine sulphate was applied preoperatively to protect the cornea during surgery, and Buprenorphine (0.05 mg/kg, Bedford Lab) was administrated as post-operative analgesic.

AAV injection and optic nerve crushing were performed as describe previously (Park et al., 2008) with minor modifications. Female C57BL6 mice (5-6 weeks old) were injected intravitreally with 2 μl volume of AAV2-GFP or AAV2-S301D paxillin-FLAG (titers at $0.5\text{-}1.0 \times 10^{13}$) to the left eyes. For each AAV injection, a glass micropipette was inserted into the peripheral retina, just behind the ora serrata, and was deliberately angled to avoid damage to the lens. Two weeks following AAV injection, the left optic nerve was exposed intraorbitally and crushed with jeweler's forceps (Dumont #5; Roboz) for 10 s approximately 1 mm behind the optic disc.

Retinal ganglion cell axon anterograde labeling

Anterograde labeling and counting of regenerating axons of retinal ganglion cells (RGCs) in mice were performed as described previously (Park et al., 2008) with minor modifications. We injected 2 μl of Alexa Fluor 555-conjugated cholera toxin B subunit (CTB) (2 μg/μl, Invitrogen) into the vitreous with a Hamilton syringe (Hamilton) to label axons anterogradely in the optic nerve. The animals were perfusion-fixed two days after CTB injection, and the number of regenerating axons was estimated by counting the number of CTB-labeled fibers extending different distances from the end of the crush site in five sections (every fourth section) per animal. Data are presented as average number of CTB-labeled axons per section extending through each distance (n=7-10 per group).

Immunofluorescence of whole mount retinas and optic nerves

Immunostaining was performed following standard protocols. All antibodies were diluted in a solution consisting of 10% normal goat serum and 1% Triton X-100 in PBS. Antibodies used were mouse anti-neuronal class p-III tubulin (clone TUJ1, 1:400 dilution, Covance), rabbit antibody against phosphorylated paxillin (1:200 dilution, Invitrogen, catalog No. 44-1028G), chicken anti-GFP (1:1,000 dilution, Abcam, catalog No. AB13970), mouse anti-FLAG (clone M2, 1:250 dilution, Sigma) and Cy2 or Cy3-conjugated secondary antibodies (1:400 dilution, Jackson).

Mouse whole mount retinas were incubated with primary antibodies overnight at 4°C and washed three times for 10 min each with PBS. Secondary antibodies were then applied and incubated for 1 h at room temperature. Tissues were again washed three times for 10 min each with PBS before a cover slip was mounted with Vectorshield (Vector). We sampled 15-20 fields randomly per retina and counted TUJ1-positive RGCs under fluorescence microscope. Because TUJ1 may also stain some non-RGC cells such as bipolar cells, only TUJ1-positive cells in the ganglion cell layer were included in this study. The average number per field of TUJ1 immunofluorescent cells in the ganglion cell layer was determined and the percentage of viable RGC number was then obtained from the value of uninjured contralateral retinas.

Optic nerves were sectioned longitudinally at 12 μm thickness and incubated sequentially with primary and secondary antibodies.

Statistical analysis

Data are expressed as the mean ± SEM. Statistical analyses were performed using Prism version 5.04 software (GraphPad). P<0.05 was judged as statistically significant.

Results

Dystrophic endballs resume forward migration after inhibition of protein kinase A

As reported previously (Tom et al., 2004), a glass coverslip was spotted with an aggrecan solution to generate a concentration gradient of aggrecan at the rim of the spot (Fig. 1A,B). Axon endings of adult rat DRG neurons formed dystrophic endballs and stopped forward migration when they encountered a rising gradient of aggrecan (Tom et al., 2004) (Fig. 1C). To investigate signaling pathways that mediate aggrecan-induced growth arrest, DRG axons were allowed to extend into the aggrecan rim in the presence of various compounds (Fig. 1C,D). These were selected based on their reported effects on axon growth, guidance or regeneration (Bradke et al., 2012; Liu et al., 2011; Tojima et al., 2011). Two different inhibitors of PKA, KT5720 and mPKI, allowed axons to migrate up the aggrecan gradient and to cross the aggrecan rim (Fig. 1C). These PKA inhibitors increased the length of axons in the rim as effectively as chondroitinase ABC that digests chondroitin sulfate chains,

although all the other compounds examined here had no detectable effect (Fig. 1D). Interestingly, KT5720 did not influence axon growth on substrates of uniform laminin or uniform aggrecan (Fig. 1E), suggesting that PKA inhibition facilitates axon growth selectively on aggrecan gradients. We next tested whether PKA inhibition can restore the growth capability of pre-formed endballs. Two days after plating, an endball was incapable of forward migration in the aggrecan rim but started to advance after KT5720 treatment (Fig. 2). Axon endings that had resumed forward migration after KT5720 treatment did not appear to be normal growth cones but retained some morphological characteristics of dystrophic endballs. To quantify endball migratory responses, we defined "migrating endballs" as those that moved forward more than 10 μm per hour. Compared to vehicle controls, treatment with either KT5720 (Table 1A) or mPKI (Table 1B) significantly increased the percentage of migrating endballs. These results indicate that PKA inhibition can reactivate the growth capability of endballs on aggrecan gradients.

PKA is activated in dystrophic endballs

The inactive PKA holoenzyme consists of two catalytic subunits bound noncovalently to two regulatory subunits (RI and RII), where RI and RII inhibit the kinase activity of catalytic subunits (Taylor et al., 1990). PKA autophosphorylation at serine 96 of RII facilitates cAMP-induced dissociation of the PKA holoenzyme, thereby enhancing PKA catalytic activity (Erlichman et al., 1983; Granot et al., 1980). As reported previously (Mizuno et al., 2002), PKA activity can be assessed using an antibody that recognizes pS^{96} PKA RII. We first validated this methodology by indirect immunofluorescence of adult rat DRG growth cones cultured on uniform laminin and pretreated with forskolin. The cells were double labeled with antibodies against pS^{96} PKA RII and total PKA RII that include both phosphorylated and non-phosphorylated PKA RII. As expected, forskolin treatment increased pS^{96} PKA RII: 132 ± 11 (arbitrary unit; n=48) and 48 ± 4 (n=36) in forskolin and vehicle-treated growth cones, respectively (P<0.001; unpaired t-test). In contrast, there was no detectable difference in total PKA RII levels: 119 ± 10 (n=48) and 137 ± 12 (n=36) in forskolin and vehicle-treated growth cones, respectively. Then, we assessed PKA RII phosphorylation in axon endings on different substrates (Fig. 3A,B). PKA RII phosphorylation in growth cones showed no significant difference between uniform laminin and uniform aggrecan. Compared to growth cones on these uniform substrates, dystrophic endballs on aggrecan gradients had increased PKA RII phosphorylation, and this was suppressed significantly by treatment with KT5720 or mPKI (Fig. 3C). These results indicate that PKA-dependent signaling is activated in dystrophic endballs on aggrecan gradients.

PKA inhibition facilitates endball migration via paxillin phosphorylation

Next we investigated a molecular pathway that links PKA to endball migration. Axon growth often relies on dynamic growth cone adhesion to the extracellular matrix, which is mediated by adhesive point contacts enriched in integrins and their interacting molecules such as paxillin (Myers et al., 2011). It is known that activation of integrin signaling promotes axon growth on uniform aggrecan substrates *in vitro* (Condic, 2001; Tan et al., 2011) and axon regeneration *in vivo* (Tan et al., 2012). These previous findings raise the possibility that endball migration also relies on intact functions of adhesive point contacts. Paxillin is a key regulator of adhesion assembly and disassembly (Deakin and Turner, 2008; Parsons et al., 2010). Paxillin phosphorylation at serine 273 in chickens, which corresponds to serine 301 in rats, promotes adhesion turnover and migration of non-neuronal cells (Nayal et al., 2006). This serine residue of paxillin is phosphorylated by p21-activated kinase (PAK) (Nayal et al., 2006), which is negatively regulated by PKA (Howe and Juliano, 2000). Therefore, we hypothesized that PKA inhibition reactivates endball migration through PAK and paxillin.

Western blot analysis of adult rat DRG neurons showed that KT5720 treatment increased immunoreactivity for pS^{301} paxillin but not for total paxillin (Fig. 4A,B), suggesting that PKA inhibition causes phosphorylation of serine 301 in paxillin. To test for the functional significance of paxillin phosphorylation, serine 301 of paxillin was substituted with either alanine (S301A paxillin) or aspartate (S301D paxillin). A previous report (Nayal et al., 2006) showed that S301A paxillin and S301D paxillin act as non-phosphorylatable and phosphomimetic forms of paxillin, respectively. Wild type or mutant paxillin cDNA was tagged with Venus cDNA and introduced into adult rat DRG neurons. Then, we measured the lengths of axons expressing the transgene to assess axon crossing of the aggrecan rim (Fig. 4C). Transfection with S301D paxillin, but not other constructs, promoted axon crossing of the rim (Fig. 4D), suggesting that paxillin phosphorylation is sufficient to induce axon growth on aggrecan gradients. We also examined the effect of KT5720 on axon growth from paxillin-transfected neurons. Whereas KT5720 treatment promoted crossing of axons that had been transfected with mock or wild type paxillin constructs, KT5720 failed to facilitate crossing of axons that expressed S301A paxillin (Fig. 4E). These results show that paxillin phosphorylation is necessary for KT5720 to stimulate axon growth on aggrecan gradients.

We further implicated S301-phosphorylated paxillin in endball migration through functional perturbation of PAK, which operates both upstream and downstream of paxillin phosphorylation: PAK is responsible for paxillin phosphorylation and also promotes adhesion turnover and cell motility in response to paxillin phosphorylation (Nayal et al., 2006). We made a kinase-inactive PAK mutant by substituting lysine 298 with alanine (K298A PAK) (Chaudhary et al., 2000; Howe and Juliano, 2000). An active form of PAK was generated by substituting threonine 422 with glutamate (T422E PAK) (Sells et al., 1997). Venus cDNA was fused to these PAK cDNAs to visualize the transgene products. Axons expressing T422E PAK extended up an aggrecan gradient more robustly than those expressing wild type or K298A PAK (Fig. 5A,B). Moreover, KT5720-induced enhancement of axon crossing of the aggrecan rim was abolished in neurons that expressed K298A PAK (Fig. 5C). These results suggest that PKA inhibition relieves endballs from aggrecan-mediated growth arrest through PAK, an enzyme associated with paxillin phosphorylation.

The resumption of endball migration is associated with increased turnover of paxillin-containing point contacts

To gain insight into how paxillin phosphorylation facilitates axon growth, we analyzed the dynamics of punctate accumulations of paxillin in axon endings by TIRF microscopy. This method was used to visualize the dynamics of adhesive point contacts on the cytoplasmic surface of growth cone plasma membrane (Woo and Gomez, 2006). We performed time-lapse imaging of growth cones on uniform laminin that expressed wild type paxillin, S301A paxillin or S301D paxillin conjugated to red fluorescent protein. Paxillin accumulations visualized as punctate fluorescent signals were continuously assembled and disassembled mostly in the periphery of growth cones. We defined the lifetime of paxillin accumulations as duration between the assembly and disassembly, and compared the lifetimes of different forms of paxillin. Accumulations of S301D paxillin had shorter lifetimes than those of wild type or S301A paxillin (Fig. 6A-C), which is consistent with the previous finding that paxillin phosphorylation increases adhesion turnover (Nayal et al., 2006). We also quantified the lifetimes of wild type paxillin accumulations in growth cones that co-expressed wild type PAK, K298A PAK or T422E PAK. The active kinase T422E PAK, which mediates paxillin phosphorylation (Nayal et al., 2006), caused a shorter lifetime of paxillin-containing point contacts than wild type PAK or K298A PAK did (Fig. 6D), further supporting the idea that paxillin phosphorylation increases point contact turnover in growth cones.

To test whether KT5720-induced resumption of endball migration on aggrecan gradients is associated with increased point contact turnover, we measured the lifetimes of paxillin accumulations in endballs and concomitantly monitored the migration speed of these endballs. In endballs transfected with wild type paxillin, KT5720 treatment shortened the lifetime of paxillin accumulations (Fig. 7A,B) and increased the speed of endball migration (Fig. 7D). In endballs expressing S301A paxillin, however, KT5720 influenced neither the lifetime of S301A paxillin accumulations (Fig. 7C) nor the speed of endball migration (Fig. 7D). Altogether, our results suggest that PKA inhibition reactivates the growth capability of endballs possibly by increasing the turnover of point contacts through paxillin phosphorylation.

Paxillin phosphorylation promotes axon growth in the injured CNS

To test whether paxillin phosphorylation promotes axon regeneration *in vivo*, we examined the effect of S301D paxillin on adult RGC axon growth in a mouse optic nerve crush model (Fig. 8A) described previously (Park et al., 2008). After optic nerve injury, CSPG are organized as a gradient with higher concentration in the lesion core and lower in the penumbra (Selles-Navarro et al., 2001). This experimental model has been used extensively to study adult CNS axon regeneration *in vivo* (Benowitz and Yin, 2008; Fischer et al., 2004; Koprivica et al., 2005; Lehmann et al., 1999; Sun et al., 2011). Intravitreal application of recombinant AAVs carrying either GFP (mock) or S301D paxillin tagged with FLAG resulted in reporter expression in more than 90% of RGCs (Fig. 8B). We estimated neuronal survival at 14 days after optic nerve crush by calculating the number of TUJ1-positive RGCs on the injured side as a percentage of that on the contralateral uninjured side: 14.2 ± 0.7% (n=5) in mock-injected retinas and 16.1 ± 1.1% (n=8) in AAV-S301D paxillin-injected retinas. The data showed no detectable difference in RGC survival between the two groups. Because endogenous paxillin phosphorylated at serine 272 (corresponding to serine 301 in rats) was detectable mostly in glial cells before and after injury to the optic nerve (Fig. 8C,D), we assessed the effect of exogenous S301D paxillin on RGC axon regeneration. Growth of S301D paxillin-transfected axons was evaluated by examining fibers labeled with the anterograde tracer CTB in the optic nerve sections across the crush site (Fig. 8E). Quantification at 14 days after injury showed an increase in CTB-labeled axons in AAV-S301D paxillin-injected mice, as compared with those in mock-injected mice, and S301D paxillin facilitated axon growth at least 0.8 mm beyond the lesion epicenter (Fig. 8F).

Discussion

We have described manipulation of intracellular signals that can reactivate the locomotive machinery of pre-formed dystrophic endballs. Axon endings on aggrecan gradients form endballs and have more active PKA than those on uniform aggrecan. Pharmacological inhibition of PKA activity enhances axon growth on aggrecan gradients but not on uniform aggrecan. More importantly, pre-formed endballs on aggrecan gradients resume forward migration after inhibition of PKA or manipulation of its downstream target paxillin, indicating that the growth arrest of endballs is reversible. This ability to remobilize stalled axon endings may be therapeutically relevant, because expression of an activated form of paxillin led to increased growth of RGC axons after optic nerve crush *in vivo*.

Whereas our results indicate that PKA inhibition facilitates endball migration on aggrecan gradients, this finding does not necessarily suggest a therapeutic potential of PKA inhibition for axon regeneration *in vivo*. Conversely, many previous studies showed that an experimental elevation of cAMP and, potentially, its consequent activation of PKA are beneficial to axon regeneration after optic nerve injury (Kurimoto et al., 2010; Monsul et al., 2004; Park et al., 2004) and spinal cord injury (Lu et al., 2004; Nikulina et al., 2004). For example, it has been suggested that cAMP cooperates with the macrophage-derived growth

factor oncomodulin to stimulate regeneration of RGC axons (Yin et al., 2006). cAMP also activates the transcription factor cAMP response element binding protein in a PKA-dependent manner, which allows adult DRG neurons to overcome hostile environments composed of myelin-associated inhibitors (Gao et al., 2004; Hannila and Filbin, 2008). In spite of these findings, the cAMP analog dibutyryl cAMP or the phosphodiesterase inhibitors 3-isobutyl-1-methylxanthine and Rolipram failed to stimulate axon crossing of inhibitory aggrecan gradients *in vitro* (Steinmetz et al., 2005), as did Sp-cAMPS and forskolin in our experiments (Fig. 1D). Moreover, pharmacological activation of the cAMP effectors PKA and Epac had no detectable effect on axon crossing of aggrecan gradients (Fig. 1D). These results strongly suggest that, unlike other regeneration blockers such as myelin-associated molecules, inhibitory proteoglycans organized as a gradient generate intracellular signals that are not abrogated by activation of cAMP effectors. One important implication is that manipulation of cAMP levels or PKA activity allows axons to overcome only some regeneration inhibitors but could even aggravate axon growth retardation caused by other inhibitors. One reasonable strategy would be to identify more specific effectors downstream of the cAMP-PKA pathway and to target these multiple effectors simultaneously such that axons could overcome multiple inhibitors. Molecular components involved in PAK-mediated paxillin phosphorylation could be a potential target in this regard.

How can PKA be activated in endballs on aggrecan gradients? Given that cAMP levels fall globally in the CNS after injury (Pearse et al., 2004), it may be unlikely that aggrecan gradients activate PKA via elevating cAMP levels although the possibility of spatially localized cAMP increases within the tip of regenerating axons cannot be excluded. Such spatial regulation of cAMP levels has been observed in hippocampal neurons after local application of brain-derived neurotrophic factor (Cheng et al., 2011). Alternatively, aggrecan gradients may regulate PKA activity in endballs independently of cAMP. For example, it is possible that A-kinase anchoring proteins (Tasken and Aandahl, 2004) mediate spatial targeting of PKA to axonal tips, as has been demonstrated in growth cone guidance of embryonic neurons (Han et al., 2007). Also, 14-3-3 proteins can downregulate PKA activity by stabilizing the interaction between regulatory and catalytic subunits of PKA for growth cone guidance (Kent et al., 2010). Similarly, several protein kinases can control PKA activity via regulating the interaction between its regulatory and catalytic subunits (Braun et al., 1991; Chaturvedi et al., 2006; Houslay, 2006).

Growth cone adhesion to the extracellular matrix is mediated, in part, by integrin-based point contacts that are 1- to 2-μm elongated or dot-like structures enriched with classical focal adhesion components such as paxillin (Myers et al., 2011). A previous report showed that paxillin is a reliable marker for growth cone point contacts (Woo and Gomez, 2006). Paxillin-containing adhesions are highly dynamic near the leading edge of growth cones (Woo and Gomez, 2006) and of non-neuronal cells (Nayal et al., 2006) and play a crucial role in cell migration. In non-neuronal cells, PAK-mediated serine phosphorylation in paxillin promotes adhesion turnover and cell migration through G protein-coupled receptor kinase interacting protein 1 (GIT1), PAK-interacting exchange factor (PIX) and PAK (Deakin and Turner, 2008). This phosphorylation event augments paxillin binding to GIT1 and promotes the localization of a GIT1-PIX-PAK complex near the leading edge (Nayal et al., 2006). PIX activates the small GTPase Rac by acting as a guanine nucleotide exchange factor. The activated Rac facilitates adhesion assembly partly through its effector PAK. Thus, PAK operates both upstream and downstream of paxillin phosphorylation, forming a positive feedback loop. Adhesion disassembly then occurs through multiple mechanisms such as GIT1-mediated sequestration of paxillin from adhesions (Zhao et al., 2000) and continued Rac activation that prevents adhesion maturation (Woo and Gomez, 2006). Our study raises the possibility that the paxillin-GIT1-PIX-PAK module or similar signaling

complexes may facilitate adhesive point contact turnover for the resumption of migration in dystrophic endballs, both *in vitro* and after injury *in vivo*. This is consistent with the observation that endballs exhibit abnormally high adhesive interactions with gradient substrates of CSPG and that peptide inhibitors of CSPG receptors prevent this over-adhesion leading to enhanced endball motility (Lang et al., 2012). Thus, CSPG receptors mediate inhibition of axon regeneration possibly through stabilization of endball adhesions, which could be relieved by interventional paxillin phosphorylation. New therapeutic targets for axon tract repair could be discovered through further investigation into molecular pathways that regulate paxillin phosphorylation as well as its downstream effector processes that reactivate adhesion dynamics and endball migration.

Acknowledgments

We thank J. Silver for his advice on endball preparations *in vitro*, H. Akiyama for his advice on statistical analyses and A.T. Guy for critical reading of this manuscript. We also thank RIKEN BSI Research Resources Center for DNA sequencing. This work was partially funded by the Uehara Memorial Foundation (H.K.), the Sumitomo Foundation (H.K.), the Mochida Memorial Foundation (H.K.), Grants-in-Aid for Scientific Research on Innovative Areas (23110005, T.T.), Scientific Research (C) (24500393, T.T.), and Young Scientists (B) (23700376, T.K.) from the Ministry of Education, Culture, Sports, Science and Technology of Japan, the Japan Science and Technology Agency PRESTO program (T.T.), the Natural Medicine and Biotechnology Research, Toyama prefecture, Japan (T.K.), and the US National Institutes of Health (HD057632, V.P.L.).

References

Aricescu AR, McKinnell IW, Halfter W, Stoker AW. Heparan sulfate proteoglycans are ligands for receptor protein tyrosine phosphatase sigma. Mol Cell Biol. 2002; 22:1881–1892. [PubMed: 11865065]

Bandtlow CE, Zimmermann DR. Proteoglycans in the developing brain: new conceptual insights for old proteins. Physiol Rev. 2000; 80:1267–1290. [PubMed: 11015614]

Benowitz L, Yin Y. Rewiring the injured CNS: lessons from the optic nerve. Exp Neurol. 2008; 209:389–398. [PubMed: 17610877]

Bradbury EJ, Moon LD, Popat RJ, King VR, Bennett GS, Patel PN, Fawcett JW, McMahon SB. Chondroitinase ABC promotes functional recovery after spinal cord injury. Nature. 2002; 416:636–640. [PubMed: 11948352]

Bradke F, Fawcett JW, Spira ME. Assembly of a new growth cone after axotomy: the precursor to axon regeneration. Nat Rev Neurosci. 2012; 13:183–193. [PubMed: 22334213]

Braun RK, Vulliet PR, Carbonaro-Hall DA, Hall FL. Phosphorylation of RII subunit and attenuation of cAMP-dependent protein kinase activity by proline-directed protein kinase. Arch Biochem Biophys. 1991; 289:187–191. [PubMed: 1654846]

Chaturvedi D, Poppleton HM, Stringfield T, Barbier A, Patel TB. Subcellular localization and biological actions of activated RSK1 are determined by its interactions with subunits of cyclic AMP-dependent protein kinase. Mol Cell Biol. 2006; 26:4586–4600. [PubMed: 16738324]

Chaudhary A, King WG, Mattaliano MD, Frost JA, Diaz B, Morrison DK, Cobb MH, Marshall MS, Brugge JS. Phosphatidylinositol 3-kinase regulates Raf1 through Pak phosphorylation of serine 338. Curr Biol. 2000; 10:551–554. [PubMed: 10801448]

Cheng PL, Song AH, Wong YH, Wang S, Zhang X, Poo MM. Self-amplifying autocrine actions of BDNF in axon development. Proc Natl Acad Sci U S A. 2011; 108:18430–18435. [PubMed: 22025720]

Condic ML. Adult neuronal regeneration induced by transgenic integrin expression. J Neurosci. 2001; 21:4782–4788. [PubMed: 11425905]

Davies SJ, Goucher DR, Doller C, Silver J. Robust regeneration of adult sensory axons in degenerating white matter of the adult rat spinal cord. J Neurosci. 1999; 19:5810–5822. [PubMed: 10407022]

Deakin NO, Turner CE. Paxillin comes of age. J Cell Sci. 2008; 121:2435–2444. [PubMed: 18650496]

Dickendesher TL, Baldwin KT, Mironova YA, Koriyama Y, Raiker SJ, Askew KL, Wood A, Geoffroy CG, Zheng B, Liepmann CD, Katagiri Y, Benowitz LI, Geller HM, Giger RJ. NgR1 and

NgR3 are receptors for chondroitin sulfate proteoglycans. Nat Neurosci. 2012; 15:703–712. [PubMed: 22406547]

Erlichman J, Rangel-Aldao R, Rosen OM. Reversible autophosphorylation of type II cAMP-dependent protein kinase: distinction between intramolecular and intermolecular reactions. Methods Enzymol. 1983; 99:176–186. [PubMed: 6316088]

Fischer D, He Z, Benowitz LI. Counteracting the Nogo receptor enhances optic nerve regeneration if retinal ganglion cells are in an active growth state. J Neurosci. 2004; 24:1646–1651. [PubMed: 14973241]

Fisher D, Xing B, Dill J, Li H, Hoang HH, Zhao Z, Yang XL, Bachoo R, Cannon S, Longo FM, Sheng M, Silver J, Li S. Leukocyte common antigen-related phosphatase is a functional receptor for chondroitin sulfate proteoglycan axon growth inhibitors. J Neurosci. 2011; 31:14051–14066. [PubMed: 21976490]

Fry EJ, Chagnon MJ, Lopez-Vales R, Tremblay ML, David S. Corticospinal tract regeneration after spinal cord injury in receptor protein tyrosine phosphatase sigma deficient mice. Glia. 2010; 58:423–433. [PubMed: 19780196]

Gao Y, Deng K, Hou J, Bryson JB, Barco A, Nikulina E, Spencer T, Mellado W, Kandel ER, Filbin MT. Activated CREB is sufficient to overcome inhibitors in myelin and promote spinal axon regeneration in vivo. Neuron. 2004; 44:609–621. [PubMed: 15541310]

Granot J, Mildvan AS, Kaiser ET. Studies of the mechanism of action and regulation of cAMP-dependent protein kinase. Arch Biochem Biophys. 1980; 205:1–17. [PubMed: 6255875]

Han J, Han L, Tiwari P, Wen Z, Zheng JQ. Spatial targeting of type II protein kinase A to filopodia mediates the regulation of growth cone guidance by cAMP. J Cell Biol. 2007; 176:101–111. [PubMed: 17200417]

Hannila SS, Filbin MT. The role of cyclic AMP signaling in promoting axonal regeneration after spinal cord injury. Exp Neurol. 2008; 209:321–332. [PubMed: 17720160]

Houslay MD. A RSK(y) relationship with promiscuous PKA. Sci STKE. 2006; 2006:pe32. [PubMed: 16926362]

Howe AK, Juliano RL. Regulation of anchorage-dependent signal transduction by protein kinase A and p21-activated kinase. Nat Cell Biol. 2000; 2:593–600. [PubMed: 10980699]

Imagama S, Sakamoto K, Tauchi R, Shinjo R, Ohgomori T, Ito Z, Zhang H, Nishida Y, Asami N, Takeshita S, Sugiura N, Watanabe H, Yamashita T, Ishiguro N, Matsuyama Y, Kadomatsu K. Keratan sulfate restricts neural plasticity after spinal cord injury. J Neurosci. 2011; 31:17091–17102. [PubMed: 22114278]

Ito Z, Sakamoto K, Imagama S, Matsuyama Y, Zhang H, Hirano K, Ando K, Yamashita T, Ishiguro N, Kadomatsu K. N-acetylglucosamine 6-O-sulfotransferase-1-deficient mice show better functional recovery after spinal cord injury. J Neurosci. 2010; 30:5937–5947. [PubMed: 20427653]

Johnson KG, Tenney AP, Ghose A, Duckworth AM, Higashi ME, Parfitt K, Marcu O, Heslip TR, Marsh JL, Schwarz TL, Flanagan JG, Van Vactor D. The HSPGs Syndecan and Dallylike bind the receptor phosphatase LAR and exert distinct effects on synaptic development. Neuron. 2006; 49:517–531. [PubMed: 16476662]

Jones LL, Tuszynski MH. Spinal cord injury elicits expression of keratan sulfate proteoglycans by macrophages, reactive microglia, and oligodendrocyte progenitors. J Neurosci. 2002; 22:4611–4624. [PubMed: 12040068]

Kamiguchi H, Yoshihara F. The role of endocytic L1 trafficking in polarized adhesion and migration of nerve growth cones. J Neurosci. 2001; 21:9194–9203. [PubMed: 11717353]

Kent CB, Shimada T, Ferraro GB, Ritter B, Yam PT, McPherson PS, Charron F, Kennedy TE, Fournier AE. 14-3-3 proteins regulate protein kinase a activity to modulate growth cone turning responses. J Neurosci. 2010; 30:14059–14067. [PubMed: 20962227]

Koprivica V, Cho KS, Park JB, Yiu G, Atwal J, Gore B, Kim JA, Lin E, Tessier-Lavigne M, Chen DF, He Z. EGFR activation mediates inhibition of axon regeneration by myelin and chondroitin sulfate proteoglycans. Science. 2005; 310:106–110. [PubMed: 16210539]

Kurimoto T, Yin Y, Omura K, Gilbert HY, Kim D, Cen LP, Moko L, Kugler S, Benowitz LI. Long-distance axon regeneration in the mature optic nerve: contributions of oncomodulin, cAMP, and pten gene deletion. J Neurosci. 2010; 30:15654–15663. [PubMed: 21084621]

Lang BT, Cregg JM, Depaul MA, Filous AR, Evans TA, Weng YL, Huang AY, Li S, Silver J. Peptide inhibitors of LAR family phosphatases release CSPG mediated entrapment of axons and promote robust behavioral recovery following contusive spinal cord injury. Soc Neurosci Abstr. 2012; 252.07

Lehmann M, Fournier A, Selles-Navarro I, Dergham P, Sebok A, Leclerc N, Tigyi G, McKerracher L. Inactivation of Rho signaling pathway promotes CNS axon regeneration. J Neurosci. 1999; 19:7537–7547. [PubMed: 10460260]

Liu K, Tedeschi A, Park KK, He Z. Neuronal intrinsic mechanisms of axon regeneration. Annu Rev Neurosci. 2011; 34:131–152. [PubMed: 21438684]

Lu P, Yang H, Jones LL, Filbin MT, Tuszynski MH. Combinatorial therapy with neurotrophins and cAMP promotes axonal regeneration beyond sites of spinal cord injury. J Neurosci. 2004; 24:6402–6409. [PubMed: 15254096]

McKeon RJ, Schreiber RC, Rudge JS, Silver J. Reduction of neurite outgrowth in a model of glial scarring following CNS injury is correlated with the expression of inhibitory molecules on reactive astrocytes. J Neurosci. 1991; 11:3398–3411. [PubMed: 1719160]

Mizuno M, Yamada K, Maekawa N, Saito K, Seishima M, Nabeshima T. CREB phosphorylation as a molecular marker of memory processing in the hippocampus for spatial learning. Behav Brain Res. 2002; 133:135–141. [PubMed: 12110446]

Monsul NT, Geisendorfer AR, Han PJ, Banik R, Pease ME, Skolasky RL Jr, Hoffman PN. Intraocular injection of dibutyryl cyclic AMP promotes axon regeneration in rat optic nerve. Exp Neurol. 2004; 186:124–133. [PubMed: 15026251]

Myers JP, Santiago-Medina M, Gomez TM. Regulation of axonal outgrowth and pathfinding by integrin-ECM interactions. Dev Neurobiol. 2011; 71:901–923. [PubMed: 21714101]

Nagai T, Ibata K, Park ES, Kubota M, Mikoshiba K, Miyawaki A. A variant of yellow fluorescent protein with fast and efficient maturation for cell-biological applications. Nat Biotechnol. 2002; 20:87–90. [PubMed: 11753368]

Nayal A, Webb DJ, Brown CM, Schaefer EM, Vicente-Manzanares M, Horwitz AR. Paxillin phosphorylation at Ser273 localizes a GIT1-PIX-PAK complex and regulates adhesion and protrusion dynamics. J Cell Biol. 2006; 173:587–589. [PubMed: 16717130]

Nikulina E, Tidwell JL, Dai HN, Bregman BS, Filbin MT. The phosphodiesterase inhibitor rolipram delivered after a spinal cord lesion promotes axonal regeneration and functional recovery. Proc Natl Acad Sci U S A. 2004; 101:8786–8790. [PubMed: 15173585]

Niwa H, Yamamura K, Miyazaki J. Efficient selection for high-expression transfectants with a novel eukaryotic vector. Gene. 1991; 108:193–199. [PubMed: 1660837]

Park K, Luo JM, Hisheh S, Harvey AR, Cui Q. Cellular mechanisms associated with spontaneous and ciliary neurotrophic factor-cAMP-induced survival and axonal regeneration of adult retinal ganglion cells. J Neurosci. 2004; 24:10806–10815. [PubMed: 15574731]

Park KK, Liu K, Hu Y, Smith PD, Wang C, Cai B, Xu B, Connolly L, Kramvis I, Sahin M, He Z. Promoting axon regeneration in the adult CNS by modulation of the PTEN/mTOR pathway. Science. 2008; 322:963–966. [PubMed: 18988856]

Parsons JT, Horwitz AR, Schwartz MA. Cell adhesion: integrating cytoskeletal dynamics and cellular tension. Nat Rev Mol Cell Biol. 2010; 11:633–643. [PubMed: 20729930]

Pearse DD, Pereira FC, Marcillo AE, Bates ML, Berrocal YA, Filbin MT, Bunge MB. cAMP and Schwann cells promote axonal growth and functional recovery after spinal cord injury. Nat Med. 2004; 10:610–616. [PubMed: 15156204]

Ramón y Cajal, S. Degeneration & regeneration of the nervous system. Oxford University Press; London: 1928.

Selles-Navarro I, Ellezam B, Fajardo R, Latour M, McKerracher L. Retinal ganglion cell and nonneuronal cell responses to a microcrush lesion of adult rat optic nerve. Exp Neurol. 2001; 167:282–289. [PubMed: 11161616]

Sells MA, Knaus UG, Bagrodia S, Ambrose DM, Bokoch GM, Chernoff J. Human p21-activated kinase (Pak1) regulates actin organization in mammalian cells. Curr Biol. 1997; 7:202–210. [PubMed: 9395435]

Shaner NC, Lin MZ, McKeown MR, Steinbach PA, Hazelwood KL, Davidson MW, Tsien RY. Improving the photostability of bright monomeric orange and red fluorescent proteins. Nat Methods. 2008; 5:545–551. [PubMed: 18454154]

Shen Y, Tenney AP, Busch SA, Horn KP, Cuascut FX, Liu K, He Z, Silver J, Flanagan JG. PTPsigma is a receptor for chondroitin sulfate proteoglycan, an inhibitor of neural regeneration. Science. 2009; 326:592–596. [PubMed: 19833921]

Silver J, Miller JH. Regeneration beyond the glial scar. Nat Rev Neurosci. 2004; 5:146–156. [PubMed: 14735117]

Steinmetz MP, Horn KP, Tom VJ, Miller JH, Busch SA, Nair D, Silver DJ, Silver J. Chronic enhancement of the intrinsic growth capacity of sensory neurons combined with the degradation of inhibitory proteoglycans allows functional regeneration of sensory axons through the dorsal root entry zone in the mammalian spinal cord. J Neurosci. 2005; 25:8066–8076. [PubMed: 16135764]

Sun F, Park KK, Belin S, Wang D, Lu T, Chen G, Zhang K, Yeung C, Feng G, Yankner BA, He Z. Sustained axon regeneration induced by co-deletion of PTEN and SOCS3. Nature. 2011; 480:372–375. [PubMed: 22056987]

Tan CL, Andrews MR, Kwok JC, Heintz TG, Gumy LF, Fassler R, Fawcett JW. Kindlin-1 enhances axon growth on inhibitory chondroitin sulfate proteoglycans and promotes sensory axon regeneration. J Neurosci. 2012; 32:7325–7335. [PubMed: 22623678]

Tan CL, Kwok JC, Patani R, Ffrench-Constant C, Chandran S, Fawcett JW. Integrin activation promotes axon growth on inhibitory chondroitin sulfate proteoglycans by enhancing integrin signaling. J Neurosci. 2011; 31:6289–6295. [PubMed: 21525268]

Tasken K, Aandahl EM. Localized effects of cAMP mediated by distinct routes of protein kinase A. Physiol Rev. 2004; 84:137–167. [PubMed: 14715913]

Taylor SS, Buechler JA, Yonemoto W. cAMP-dependent protein kinase: framework for a diverse family of regulatory enzymes. Annu Rev Biochem. 1990; 59:971–1005. [PubMed: 2165385]

Tojima T, Hines JH, Henley JR, Kamiguchi H. Second messengers and membrane trafficking direct and organize growth cone steering. Nat Rev Neurosci. 2011; 12:191–203. [PubMed: 21386859]

Tom VJ, Steinmetz MP, Miller JH, Doller CM, Silver J. Studies on the development and behavior of the dystrophic growth cone, the hallmark of regeneration failure, in an in vitro model of the glial scar and after spinal cord injury. J Neurosci. 2004; 24:6531–6539. [PubMed: 15269264]

Van Vactor D, Wall DP, Johnson KG. Heparan sulfate proteoglycans and the emergence of neuronal connectivity. Curr Opin Neurobiol. 2006; 16:40–51. [PubMed: 16417999]

Woo S, Gomez TM. Rac1 and RhoA promote neurite outgrowth through formation and stabilization of growth cone point contacts. J Neurosci. 2006; 26:1418–1428. [PubMed: 16452665]

Yin Y, Henzl MT, Lorber B, Nakazawa T, Thomas TT, Jiang F, Langer R, Benowitz LI. Oncomodulin is a macrophage-derived signal for axon regeneration in retinal ganglion cells. Nat Neurosci. 2006; 9:843–852. [PubMed: 16699509]

Yiu G, He Z. Glial inhibition of CNS axon regeneration. Nat Rev Neurosci. 2006; 7:617–627. [PubMed: 16858390]

Zhao ZS, Manser E, Loo TH, Lim L. Coupling of PAK-interacting exchange factor PIX to GIT1 promotes focal complex disassembly. Mol Cell Biol. 2000; 20:6354–6363. [PubMed: 10938112]

Highlights

- Inhibitory proteoglycan gradients cause PKA activation in dystrophic endballs.
- PKA inhibition restores the growth capability of dystrophic endballs.
- Endballs resume forward migration possibly through increased adhesion dynamics.
- Serine phosphorylation on paxillin mediates resumption of endball migration.
- Paxillin phosphorylation promotes axon growth in the injured CNS.

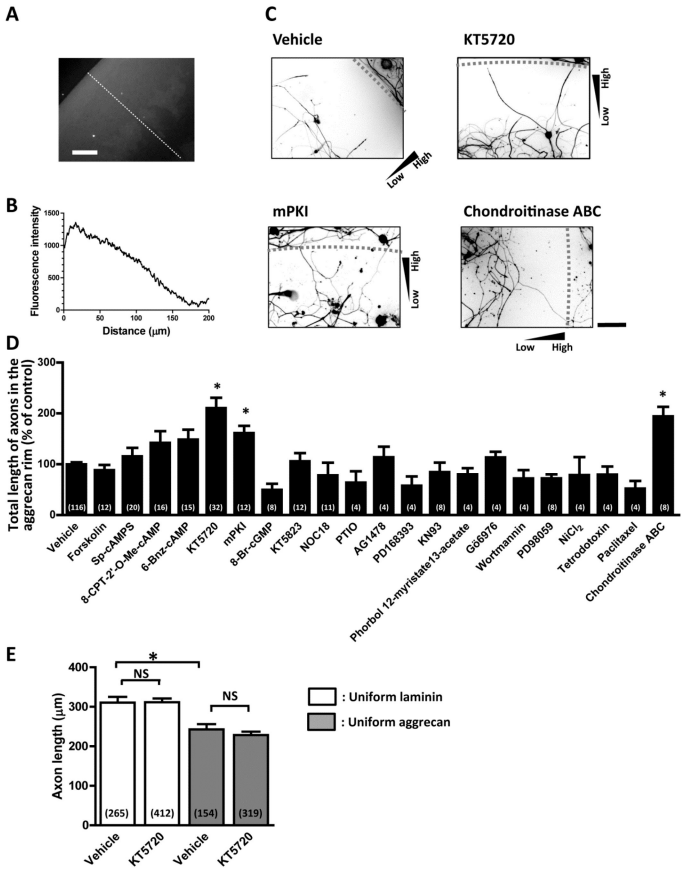

Fig. 1.

PKA Inhibitors facilitate axon growth on aggrecan gradients. A. An aggrecan gradient visualized with the anti-chondroitin sulfate antibody CS-56. Scale bar, 50 μm. B. Line profile of fluorescence intensity along the dashed line in (A). The x-axis represents distance in microns from the outer boundary of aggrecan rim. C. Adult DRG neurons labeled for β tubulin III. Cultures were maintained in the absence (vehicle only) or presence of PKA inhibitors, KT5720 and mPKI, and chondroitinase ABC. Each triangle indicates the direction of an aggrecan gradient. Dashed lines represent the outer boundary of aggrecan rims. Scale bar, 100 μm. D. Quantification of axon crossing of the aggrecan rim. The vertical axis represents the sum of lengths of all axonal segments in the rim. The effect of the following compounds was examined: forskolin (adenylate cyclase activator), Sp-cAMPS (cAMP analog), 8-CPT-2′-O-Me-cAMP (Epac activator), 6-Bnz-cAMP (PKA activator), KT5720, mPKI, 8-Br-cGMP (cGMP analog), KT5823 (protein kinase G inhibitor), NOC18 (nitric oxide donor), PTIO (nitric oxide scavenger), AG1478 and PD168393 (epidermal growth factor receptor inhibitors), KN93 (calcium/calmodulin-dependent protein kinase inhibitor), phorbol 12-myristate 13-acetate (protein kinase C activator), Gö6976 (protein kinase C inhibitor), wortmannin (phosphoinositide 3-kinase inhibitor), PD98059 (mitogen-activated protein kinase kinase inhibitor), $NiCl_2$ (voltage-gated calcium channel blocker), tetrodotoxin (sodium channel blocker), paclitaxel (microtubule stabilizer) and chondroitinase ABC. Numbers in parentheses indicate the total number of aggrecan spots examined. *P<0.05 versus vehicle; Bonferroni's multiple comparison test. E. Quantification of axon growth on uniform substrates of laminin or aggrecan. After treatment with KT5720 or vehicle only, length of the longest axon in each neuron was measured. Numbers in parentheses indicate the total number of neurons examined. *P<0.05; NS, not significant; Bonferroni's multiple comparison test.

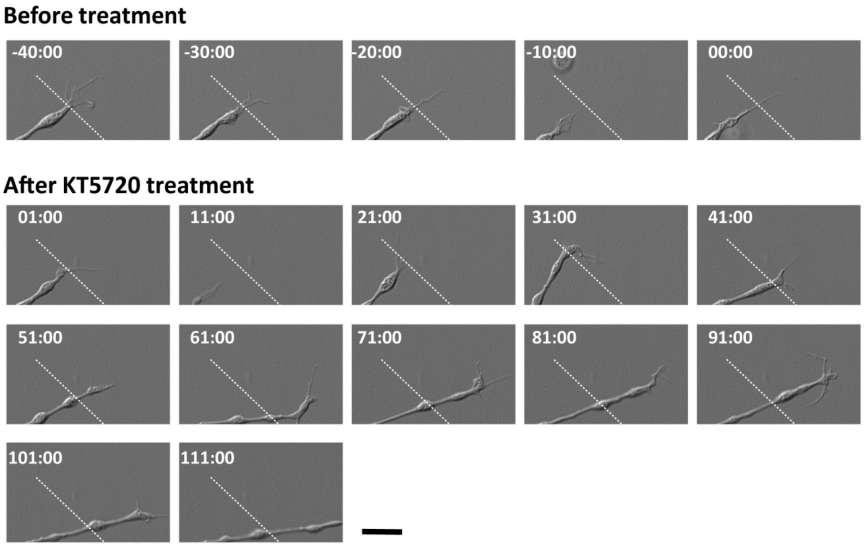

Fig. 2.

A pre-formed endball resumes forward migration after PKA inhibition. Shown are time-lapse DIC images of an endball on an aggrecan gradient before and after KT5720 treatment. Digits represent minute:second after bath application of KT5720. Dashed lines represent the position of endball tip at -40:00. Scale bar, 10 μm.

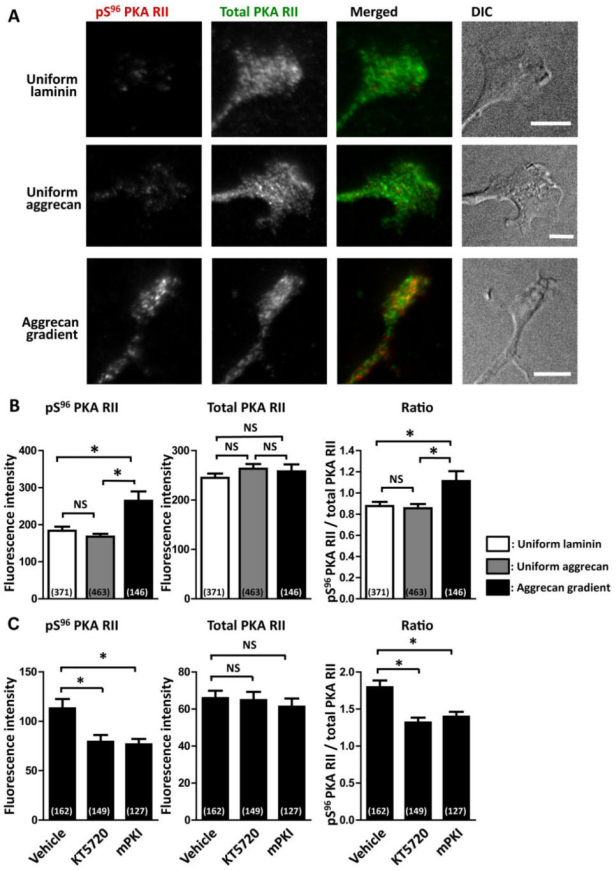

Fig. 3.

Increased PKA phosphorylation in dystrophic endballs on aggrecan gradients. A. Axon endings on uniform substrates of laminin or aggrecan and gradient substrates of aggrecan were double labeled for pS^{96} PKA RII (red) and total PKA RII (green). Scale bars, 10 μm. B,C. Fluorescence intensities of pS^{96} PKA RII and total PKA RII in axon endings were measured, and ratios of pS^{96} PKA RII to total PKA RII were calculated. C. The effect of PKA inhibitors, KT5720 or mPKI, on PKA phosphorylation was examined in axon endings on aggrecan gradients. Numbers in parentheses indicate the total number of axons examined. *P<0.05; NS, not significant; Bonferroni's multiple comparison test.

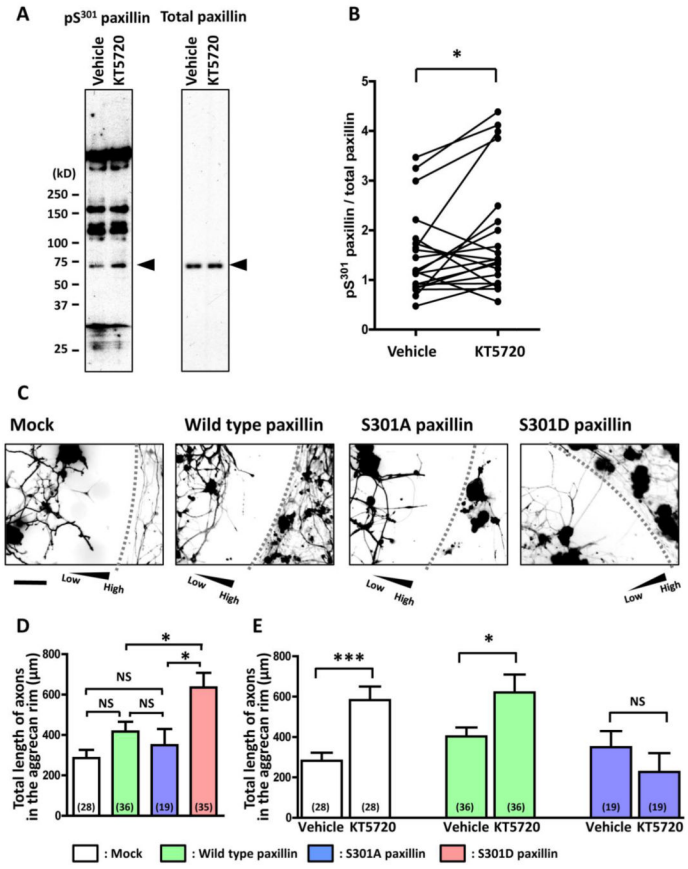

Fig. 4.

PKA inhibition facilitates axon crossing of aggrecan gradients through paxillin phosphorylation. A. Western blot analysis of cultured DRG neurons treated with KT5720 or vehicle only. Arrowheads indicate paxillin bands. Blots were first probed with anti-pS^{301} paxillin antibody and then stripped and reprobed with anti-total paxillin antibody. B. Quantification of Western blot intensities. Ratios of pS^{301} paxillin to total paxillin were determined. A pair of two blots (KT5720 or vehicle treatment) in each gel was compared. *P<0.05; paired t-test. C. Fluorescence images of DRG neurons expressing Venus (mock) or Venus-conjugated wild type or mutant paxillin. Each triangle indicates the direction of an aggrecan gradient. Dashed lines represent the outer boundary of aggrecan rims. Scale bar, 100 μm. D. The effect of paxillin transfection on axon crossing of the aggrecan rim. Axons expressing wild type paxillin (green), S301A paxillin (blue) and S301D paxillin (red) were analyzed. The vertical axis represents the sum of lengths of all axonal segments in the rim. Numbers in parentheses indicate the total number of aggrecan spots examined. *P<0.05; NS, not significant; Bonferroni's multiple comparison test. E. The effect of KT5720 on axon crossing of the aggrecan rim. KT5720 failed to promote axon crossing in neurons expressing S301A paxillin. *P<0.05, ***P<0.001; NS, not significant; unpaired t-test.

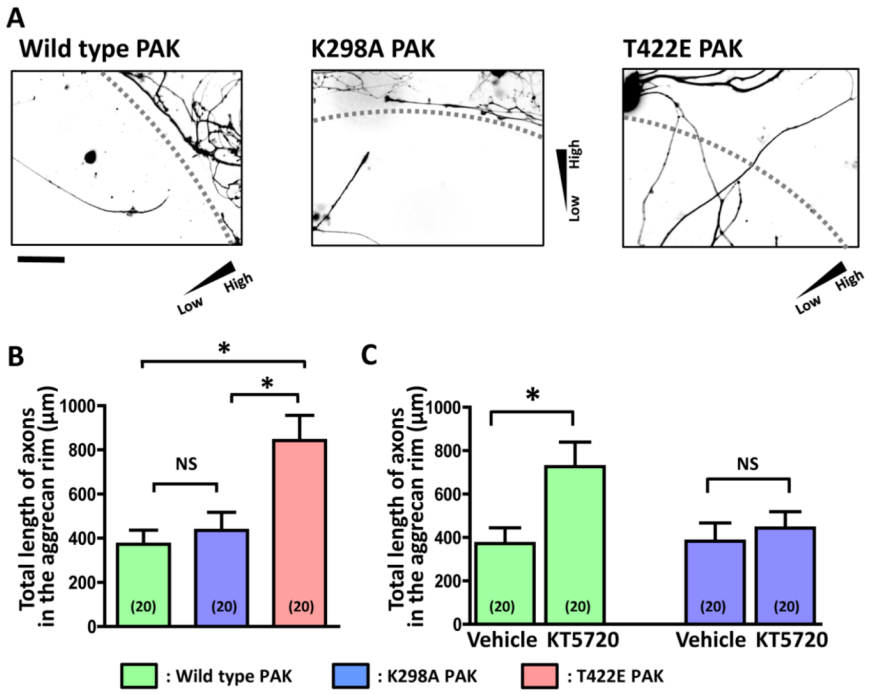

Fig. 5.

The active form of PAK facilitates axon crossing of aggrecan gradients. A. Fluorescence images of DRG neurons expressing Venus-conjugated wild type or mutant PAK. Each triangle indicates the direction of an aggrecan gradient. Dashed lines represent the outer boundary of aggrecan rims. Scale bar, 100 μm. B. The effect of PAK transfection on axon crossing of the aggrecan rim. Axons expressing wild type PAK (green), K298A PAK (blue) and T422E PAK (red) were analyzed. The vertical axis represents the sum of lengths of all axonal segments in the rim. Numbers in parentheses indicate the total number of aggrecan spots examined. *P<0.05; NS, not significant; Bonferroni's multiple comparison test. C. The effect of KT5720 on axon crossing of the aggrecan rim. KT5720 failed to promote axon crossing if neurons expressed K298A PAK. *P<0.05; NS, not significant; unpaired t-test.

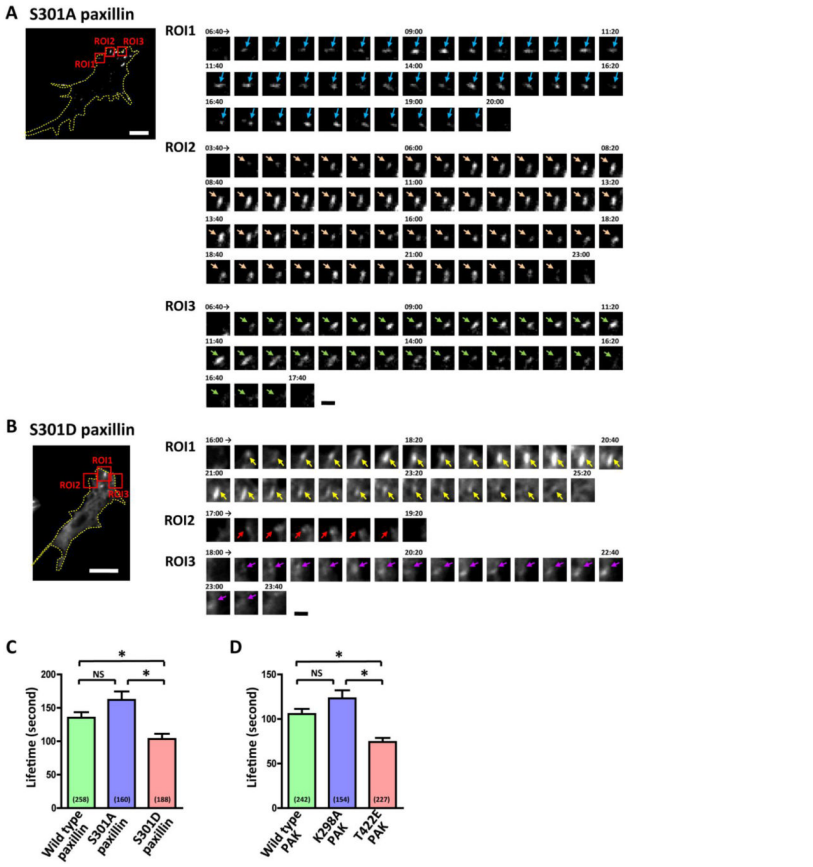

Fig. 6.

The lifetime of paxillin-containing point contacts in growth cones on uniform laminin. A, B. TIRF images of TagRFP-T-conjugated S301A paxillin (A) or S301D paxillin (B) expressed in growth cones. The yellow dotted lines represent the growth cone outlines. The red boxes represent regions of interest (ROIs) showing time sequence of paxillin accumulation. Arrows of each color indicate a single paxillin accumulation. Digits represent minute:second. White scale bars, 5 μm. Black scale bars, 1 μm. C. The lifetime of accumulations of TagRFP-T-conjugated wild type or mutant paxillin in growth cones. Numbers in parentheses indicate the total number of accumulations examined. **P*<0.05; NS, not significant; Bonferroni's multiple comparison test. D. To examine the effect of wild type, K298A or T422E PAK on the lifetime of paxillin-containing point contacts, DRG neurons were doubly transfected with these forms of PAK and TagRFP-T-conjugated wild type paxillin. The graph shows the lifetime of accumulations of TagRFP-T-conjugated wild type paxillin in growth cones. **P*<0.05; NS, not significant; Bonferroni's multiple comparison test.

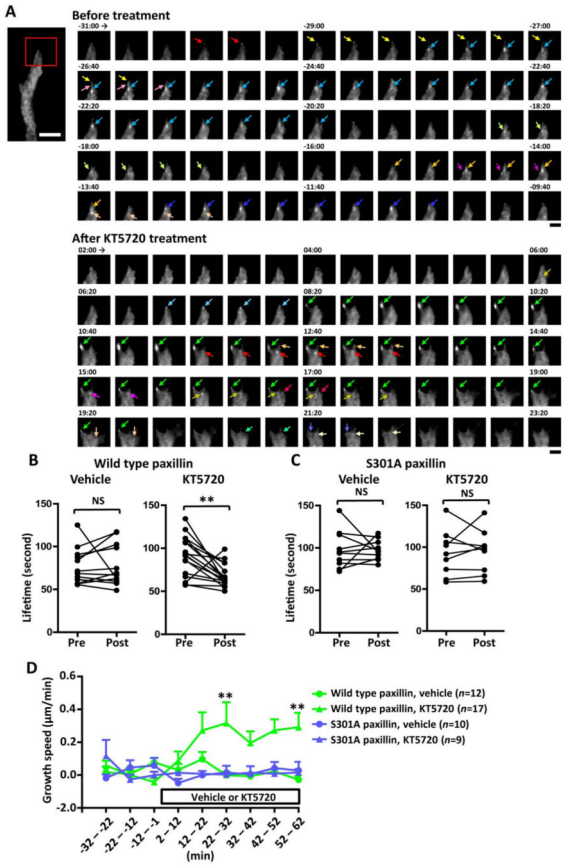

Fig. 7.

Resumption of endball migration is associated with increased point contact turnover. A. TIRF images of TagRFP-T-conjugated wild type paxillin expressed in a dystrophic endball on an aggrecan gradient. Shown are time-lapse images of paxillin accumulations in the red squared area before and after bath application of KT5720. Arrows of each color indicate a single paxillin accumulation. Digits represent minute:second after application of KT5720. Each colored arrow indicates a single paxillin accumulation. White scale bar, 5 μm. Black scale bars, 2 μm. B,C. The effect of KT5720 or vehicle only on the lifetime of accumulations of TagRFP-T conjugated to wild type paxillin (B) or S301A paxillin (C). Each closed circle represents the mean lifetime in a single endball from −31 to −1 min (pre) and from 2 to 32 min (post) after the onset of pharmacological treatment. $^{**}P<0.01$; NS, not significant; paired *t*-test. D. Growth speeds of the axons analyzed in (B) and (C). Each plot represents the average speed during the indicated 10-min intervals of axons that expressed TagRFP-T-conjugated wild type paxillin (green) or S301A paxillin (blue) and were treated with KT5720 (triangle) or vehicle only (circle). The pharmacological treatment started at 0 min. Two-way ANOVA with repeated measures showed that the speed is affected significantly by the two factors “pharmacological reagent” ($P<0.05$) and “time” ($P<0.05$) as well as their interaction ($P<0.01$). $^{**}P<0.01$ versus vehicle-treated, wild type paxillin-transfected axons during the same time interval; Bonferroni's multiple comparison test.

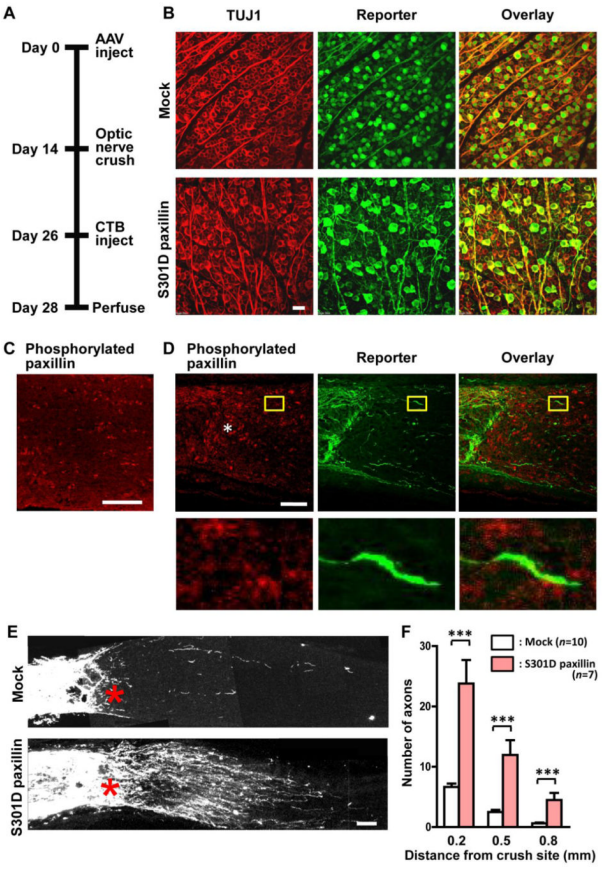

Fig. 8.

S301D paxillin facilitates RGC axon growth after optic nerve injury. A. Scheme of the experimental protocol used to evaluate the effect of intravitreal AAV application on RGC survival and regeneration. B. Retinas injected with AAV-GFP (mock) or AAV-S301D paxillin were double labeled for β tubulin III (TUJ1) and a reporter (GFP or FLAG). Confocal images of the ganglion cell layer are shown. Scale bar, 20 μm. C. Immunofluorescence of phosphorylated paxillin in an uninjured optic nerve. A longitudinal confocal section is shown. Scale bar, 100 μm. D. Immunofluorescence of phosphorylated paxillin and GFP in a mock-injected optic nerve around the crush site (asterisk) at 14 days after injury. Magnified views of the areas of interest (rectangles) are shown below the corresponding images. Scale bar, 100 μm. E. Confocal images of optic nerves of different AAV-injected groups, showing CTB-labeled axons around the crush sites (red asterisks) at 14 days after injury. Each panel is a composite of multiple fluorescent images acquired under the same optical conditions. Scale bar, 100 μm. F. Quantification of growing axons counted at 0.2, 0.5 and 0.8 mm distal to the crush site. ***P<0.001; unpaired t-test.

Table 1

The number and percentage of endballs that showed each migratory response to PKA inhibition.

A

	No migration	Resumed migration
Vehicle	41 (83.7%)	8 (16.3%)
KT5720	33 (43.4%)	43 (56.6%)

$P < 0.0001$, Fisher's exact test

B

	No migration	Resumed migration
Vehicle	26 (89.6%)	3 (10.3%)
mPKI	21 (53.8%)	18 (46.1%)

$P < 0.01$, Fisher's exact test